



Fermi National Accelerator Laboratory

FERMILAB-Conf-91/193-E

## Jets in CDF

E. Buckley-Geer

*Rutgers University*

The CDF Collaboration

*Fermi National Accelerator Laboratory  
P.O. Box 500, Batavia, Illinois 60510*

July 1991

\* Presented at the *VI Conference on Intersections of Particle and Nuclear Physics*, Tuscon, Arizona, May 24-29, 1991.

## JETS IN CDF

Elizabeth Buckley-Geer  
Rutgers University  
CDF Collaboration

## ABSTRACT

In the 1988/89 Tevatron Collider run the CDF experiment collected  $4.0 \pm 0.3$  pb<sup>-1</sup> of proton-antiproton interactions at a center-of-mass energy of 1800 GeV. This is the highest proton-antiproton center-of-mass collision energy currently available in the laboratory and gives us a unique opportunity for studying Quantum Chromodynamics (QCD) processes at the highest available energies. We report results from various QCD studies performed with this data.

## WHAT IS A JET IN CDF?

The CDF detector had been described in detail elsewhere<sup>1</sup>. We will describe briefly the parts of the detector that are relevant for the measurements presented here. A system of eight vertex time-projection (VTPC) chambers surround the interaction region out to angles greater than  $3.5^\circ$  from the beam axis and provide an accurate determination of the interaction vertex. Around the VTPC is the central tracking chamber (CTC) that provides precision momentum determination of charged particles by curvature in a uniform 1.4 Tesla solenoidal magnetic field. It covers the pseudorapidity interval  $|\eta| < 1$  ( $\eta = \ln(\tan \theta/2)$ ). The calorimeters are located outside the magnet coil and cover the region  $|\eta| < 4.2$ . They are segmented into projective towers of 0.1 units in  $\eta$  and  $15^\circ$  in azimuth ( $|\eta| < 1.3$ ) and  $5^\circ$  in azimuth at larger  $\eta$ . They consist of an electromagnetic section whose radiator is lead and a hadronic section whose radiator is iron. In the central part ( $|\eta| < 1.3$ ) the active medium is plates of scintillator. At larger pseudorapidity the active medium is gas proportional tubes.

Jets are reconstructed using a cone algorithm in  $\eta$ - $\phi$  space. The radius of the cone is defined as  $\Delta R = \sqrt{(\Delta\eta)^2 + (\Delta\phi)^2}$  where  $\Delta\eta$  is the distance in pseudorapidity between the centroid of a calorimeter cell and the jet axis and  $\Delta\phi$  is the corresponding distance in azimuth. The energy and momentum of the jet are defined as follows

$$E_J = \sum_{i=1}^N E_i, \quad \mathbf{P}_J = \sum_{i=1}^N \mathbf{P}_i$$

The angle of the jet centroid with respect to the beam direction is defined as  $\sin \theta_J = P_T/P_J$  and the jet transverse energy is given by  $E_T = E_J \sin \theta_J$ . We use a cone radius of 0.7 unless stated otherwise.

Typically, jet  $E_T \neq$  parton  $E_T$  for a number of reasons. Energy is lost in uninstrumented parts of the detector such as cracks, energy from the underlying event contributes to the energy inside the jet cone and energy falling outside the cone due to fragmentation effects. We correct for the first two effects but not the third as this makes comparisons to next-to-leading order calculations difficult.

Presented at the VI Conference on Intersections of Particle and Nuclear Physics, Tuscon, Arizona, May 24-29 1991.

## MEASUREMENT OF THE INCLUSIVE JET CROSS-SECTION

Recently, calculations at next-to-leading order ( $O(\alpha_s^3)$ ) have become available<sup>2,3,4</sup>. These calculations make predictions for the inclusive jet cross-section which depend on the cone size used for jet clustering. In addition, the  $O(\alpha_s^3)$  has a reduced dependence on the renormalization scale  $\mu$ , for a cone size of 0.7 the uncertainty on the calculation is about 10%.

Jets were required to have a pseudorapidity in the range  $0.1 < |\eta| < 0.7$  and  $E_T > 35$  GeV. Cosmic rays were removed by use of an appropriate algorithm. The resulting spectrum is shown in figure 1. The data have been corrected for the effects of the calorimeter response and energy losses. The error bars represent the statistical and  $E_T$ -dependent systematic uncertainties added in quadrature. An overall normalization uncertainty is also shown. The total

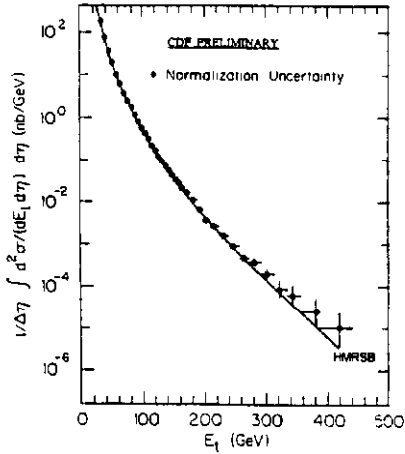


Fig. 1 Inclusive jet  $E_T$  spectrum.

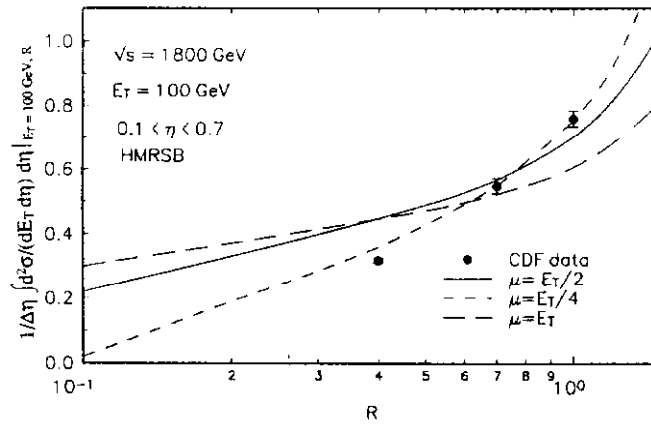


Fig. 2 Dependence of the cross-section on cone size for  $E_T = 100$  GeV

systematic uncertainty for  $E_T > 84$  GeV is about 23%. The curve is an  $O(\alpha_s^3)$  prediction<sup>4</sup> using HMRSB structure function<sup>5</sup> and  $\mu = P_T$ . The agreement is impressive over seven orders of magnitude (the normalization is absolute). Figure 2 shows the measured cross-section for  $E_T = 100$  GeV at three different cone sizes, 0.4, 0.7 and 1.0. Also shown are the predictions from the next-to-leading order calculation<sup>6</sup> for three values of the renormalization scale  $\mu$ . The slope of the data at  $R=0.7$  is  $0.70 \pm 0.05$  nb/GeV which compares well with the  $O(\alpha_s^3)$  prediction of  $0.5 \pm 0.2$  nb/GeV. We note that there seems to be a minimum dependence on the renormalization scale for a cone size of 0.7.

### $P_T$ FLOW ABOUT THE JET AXIS

Another consequence of the  $O(\alpha_s^3)$  calculations is that they make predictions for the the  $P_T$  flow about the jet axis as there is now the possibility of having two partons in the clustering cone.

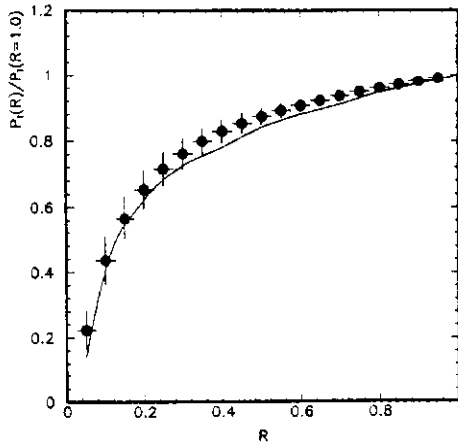


Fig. 3  $P_T$  flow about the jet axis.

Jets were selected with pseudorapidity in the range  $0.1 < |\eta| < 0.7$  and  $95 \text{ GeV} < E_T < 120 \text{ GeV}$  after correction. The  $P_T$  flow in a cone of radius  $R$  is defined as the sum of the charged tracks within that cone

$$P_T(R) = \frac{1}{N} \sum_N \int_0^R \frac{dP_T}{dr} dr.$$

Various quality cuts are applied that select good 3-dimensional tracks. The jet axis is defined using the calorimeter information and a clustering cone of 1.0 so that most of the jet energy is contained. The data have been corrected for the loss of tracking efficiency in the core of jets. This correction is 7% near the jet core and negligible elsewhere. The distribution  $P_T(R)/P_T(R=1.0)$  is shown in figure 3. The error bars represent the statistical plus systematic uncertainties added in quadrature. The  $\alpha_s^3$  calculation is by S. Ellis et al.<sup>7</sup> with HMRSB structure functions<sup>8</sup> and  $\mu = P_T/2$ . The data are reasonably well described, indicating that the  $P_T$  flow within the jet appears to be dominated by the gluon radiation not by the fragmentation. However we note here that other choices for  $\mu$  give less good agreement.

### TWO-JET MASS SPECTRUM

Another test of QCD is the measurement of the mass spectrum for two-jet events. The mass spectrum is sensitive to resonant production of a new particle decaying into two jets, e.g., axiguons. The comparison with theory is presently limited to lowest order ( $\alpha_s^2$ ) but  $O(\alpha_s^3)$  calculations are in progress.

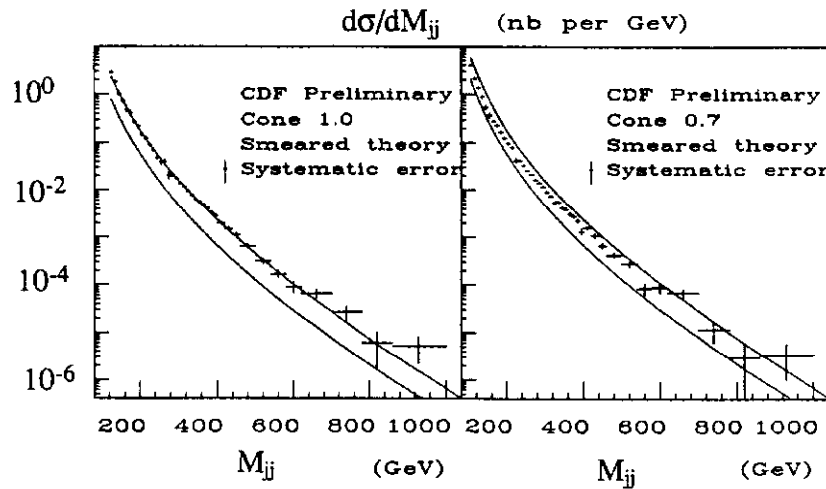


Fig. 4 Two-jet mass spectrum for cone sizes of 1.0 and 0.7.

The event selection requires at least two clusters with  $|\eta_1|, |\eta_2| < 0.7$ . Cosmic rays are removed using an appropriate algorithm. Jet clustering cones of 1.0 and 0.7 were used. The jet energies are corrected for losses and underlying event but not energy outside the clustering cone. In order to compare the theory to the data we have convoluted the theoretical spectrum with the measured calorimeter response, rather than unsmear the data.

Figure 4 shows the resulting spectrum for the two cone sizes. The errors are statistical only and the average systematic uncertainty is indicated by the error bar. The band represents the spread of theoretical predictions using a variety of structure functions and Q-scales (the scale is absolute).

In order to determine how well the shape agrees we allow the normalization to float and the theory curves are fitted to the data. We find that the quality of the fits is almost independent of the choice of Q-scale and not very sensitive to the choice of structure function. The spectrum obtained with the cone of 1.0 is well described by all structure functions and Q-scales (with the exception of EHLQ2). However, the spectrum for the cone of 0.7 has a different shape from the cone of 1.0 and is not well described by any of the choices. We have investigated to see whether this difference in shape could be due to a different calorimeter response between the two cone sizes but we see no evidence for this. If we correct the  $R=0.7$  spectrum for the energy lost outside the clustering cone then the shape difference is reduced but not eliminated. We await the  $O(\alpha_s^3)$  calculation to see if this can explain the difference.

### THREE-JET KINEMATICS

We are able to make a high-statistics comparison of the three-jet kinematics with leading-order QCD ( $O(\alpha_s^3)$ ) predictions. We adopt the variables defined by the UA1 collaboration<sup>9</sup>.

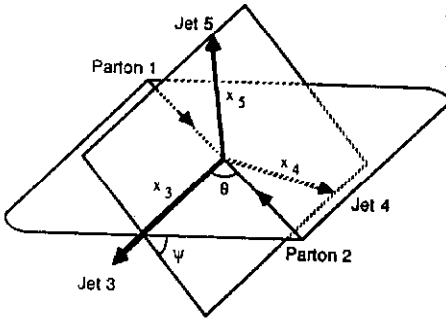


Fig. 5 Three-jet kinematics

Figure 5 shows a three-jet event in the center-of-mass frame of the three jets. There are four independent variables that describe the event:-

(i) the energy fractions  $x_3$  and  $x_4$ , where  $x_i = 2E_i/M_{3J}$  and  $M_{3J}$  is the three-jet invariant mass. The  $x_i$ s satisfy the conditions  $x_3 + x_4 + x_5 = 2$  and  $x_3 > x_4 > x_5$ ,

(ii)  $\cos \theta_3$ , which is the angle between Jet-3 and the incoming partons,

(iii)  $\psi$ , which is the angle between the plane containing jet-3 and the incoming partons and the plane containing Jet-4 and Jet-5.

Events were required to pass the following selection cuts. At least three clusters with  $E_T > 10$  GeV,

$|\eta_{\text{detector}}| < 3.5$  and separation between the jets in  $\eta$ - $\phi$  space of at least 0.85. In addition, cuts were made on the kinematic variables to ensure good acceptance. These were  $x_3 < 0.9$ ,  $\cos \theta_3 < 0.6$ ,  $150^\circ > |\psi| > 30^\circ$  and  $M_{3J} > 250$  GeV/ $c^2$ . The distributions for  $x_3$  and  $x_4$  are shown in figure 6 along with the predictions from phase-space (constant matrix element), full QCD and  $q\bar{q}$  initial states only. The data clearly prefer the full QCD curve. The enhancement at large  $x_3$  is due to the increase in cross-section for events that have a soft third jet. Also shown in figure 7 are the distributions

for  $\cos \theta_3$  and  $\psi$ , with the same set of curves. Again the data prefer the full QCD curve. The forward peaking in the  $\cos \theta_3$  distribution is characteristic of t-channel exchange processes such as  $gg \rightarrow gg$ . The peaking in the  $\psi$  distribution arises because of the increased cross-section for events where Jet-5 is close to the incoming parton.

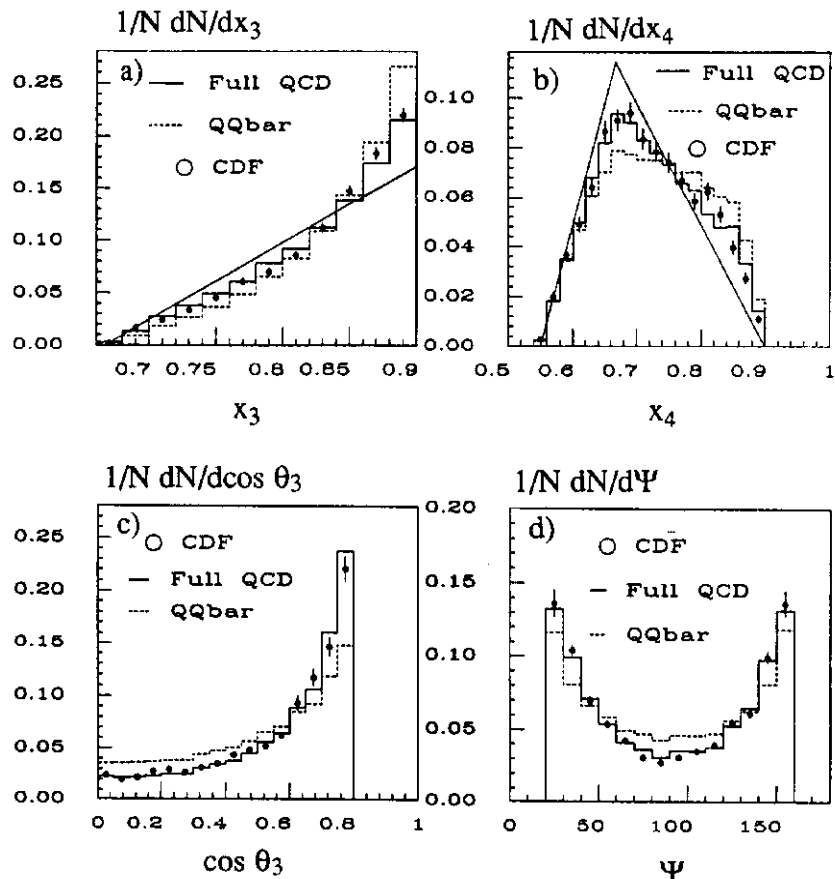


Fig. 7 Kinematic distributions for three-jet events. a)  $x_3$ , b)  $x_4$ , c)  $\cos \theta_3$  d)  $\psi$ .

### HIGH TOTAL TRANSVERSE ENERGY EVENTS

This study is somewhat different compared to the others described here because it makes no assumptions about the jet structure of the events. Instead, events are selected by requiring total transverse energy  $\Sigma E_T$  in excess of 400 GeV, where

$$\Sigma E_T = \sum_i E_i \sin \theta_i$$

and  $E_i$  is the energy of the  $i$ th calorimeter cell and  $\theta_i$  is the angle between the  $i$ th cell and the beam direction. The sum is over all cells with  $E_T > 500$  MeV. In addition, we require that the total energy seen by the calorimeters is less than 2000 GeV, that the

missing transverse-energy significance ( $S = \cancel{E}_T / \sqrt{\Sigma E_T}$ ) is less than 6 and that there be no second vertex reconstructed in the VTPC with  $> 10$  tracks separated from the primary vertex by more than 10 cm. We also remove cosmic rays. The final sample consists of 279 events.

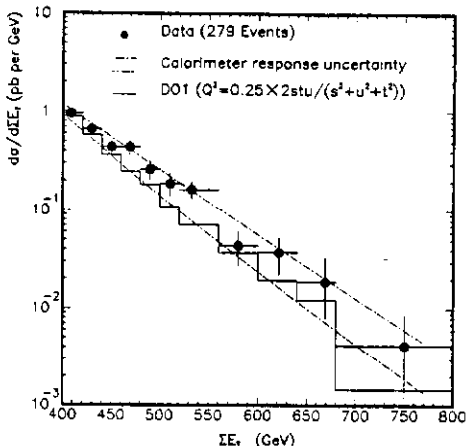


Fig. 8 Cross-section  $d\sigma/d\Sigma E_T$  versus  $\Sigma E_T$ .

We use the Herwig Monte Carlo (version 4.3)<sup>10</sup> plus the CDF detector simulation for the QCD comparison. We have studied distributions of jet  $P_T$ , jet  $\eta$ , jet multiplicity, jet profiles in  $\eta$  and  $\phi$ , jet widths in  $\eta$  and  $\phi$ , multi-jet mass and we find that Herwig does a reasonable job of describing them all. There is no evidence for an excess of isolated high- $P_T$  leptons or photons in the data, nor is there any excess of fat jets, thin jets or massive jets. Figure 8 shows the differential cross-section  $d\sigma/d\Sigma E_T$  as a function of  $\Sigma E_T$ . The solid curve is the prediction from Herwig plus detector simulation with the DO1<sup>11</sup> structure function and  $Q^2 = 0.25 \times 2stu/(s^2+t^2+u^2)$ . The normalization is absolute. The dashed lines indicate the uncertainty on the data arising from

the uncertainty in the calorimeter response.

## SUMMARY

We have studied a large number of different QCD processes and the indications are that at high energies QCD works well. The next-to-leading order calculations that are now appearing mean that much more precise tests of QCD can be made than were previously possible. There is no evidence for deviations from the Standard Model at the present time.

## REFERENCES

1. F. Abe et al. (CDF Collaboration), Nucl. Instr. and Meth. A271 (1988) 387.
2. R. Ellis and J. Sexton, Nucl. Phys. B269 (1986) 445.
3. F. Aversa et al., Phys. Lett. B210 (1988) 225.
4. S. Ellis, Z. Kunszt and D. Soper, Phys. Rev. Lett. 62 (1989) 2188.
5. A. Martin, R. Roberts and W. Stirling, Phys. Rev. D37 (1988) 1161.
6. S. Ellis and D. Soper, private communication (1991).
7. S. Ellis, private communication (1991).
8. P. Harriman, A. Martin, R. Roberts and W. Stirling,
9. G. Arnison et al., Phys. Lett. 158B (1985) 494.
10. G. Marchesini and B.R. Webber, Nucl. Phys. B310 461 (1988).
11. D.W. Duke and J.F. Owens, Phys. Rev. D30 49 (1984).